Vortex dynamics in cubic-quintic Bose-Einstein condensates

T. Mithun,[1] K. Porsezian,[1] and Bishwajyoti Dey[2]
[1]*Department of Physics, Pondicherry University, Puducherry 605014, India*
[2]*Department of Physics, University of Pune, Pune 411007, India*
(Received 6 March 2013; revised manuscript received 11 May 2013; published 8 July 2013)

We study vortex dynamics in a trapped Bose-Einstein condensate with tunable two- and three-body interactions. The dynamics is governed by two-dimensional cubic-quintic Gross-Pitaevskii equation. A time-dependent variational method has been used to obtain critical rotational frequency and surface mode frequency analytically and are compared with numerical simulation results. An imaginary time propagation method and Crank-Nicolson scheme for discretization have been used for numerical simulation. The numerically calculated average value of the angular momentum per particle shows very clearly its dynamical relation with the time development of the vortex formation. The rotational frequency dependence of the variation of average value of the angular momentum per particle with time shows that vortices form much faster in time for higher rotational frequency. Similarly, the vortex forms much faster in time with an increase of the strength of the repulsive three-body interaction. The simulation of the vortex lattice formation in the condensate shows that the presence of the three-body interactions does not alter the vortex lattice pattern but it helps in the shape deformations of the condensate thereby leading to vortex lattice formation. Likewise, the three-body interactions enable the vortex lattice formation in Bose-Einstein condensates even with attractive two-body interactions and in purely quintic BEC.

DOI: 10.1103/PhysRevE.88.012904 PACS number(s): 05.45.−a, 03.75.Lm

I. INTRODUCTION

Following theoretical developments, the experimental realization of Bose-Einstein condensates (BECs) of alkali-metal atoms have provided a new leap in the field of atomic physics. It opened wide the opportunity to explore many properties of atomic clouds, especially collective excitations such as vortices [1–3], solitons, mode coupling [4,5], nonlinear interferometry [6], etc., of cold atoms. Exact vortex soliton solutions in quasi-two-dimensional BEC with cubic-quintic nonlinearity has been obtained recently [7]. Two classes of vortex solitons and their stability in quasi-two-dimensional BEC with cubic-quintic nonlinearity has also been obtained recently [8]. The theoretical developments of the study of vortices in superfluids started with the work of Landau in 1941 [9,10]. Later it has been found that techniques such as rotating the trap or rotating the laser beam or Raman transitions scheme can be utilized for vortex creation and there is a minimum rotational frequency for vortex nucleation [11]. Since its experimental realization, the comparison between the experimental and theoretical values of critical rotational frequency Ω_c, for the harmonically as well as the anharmonically trapped condensate have taken place [12–14]. Also it has been observed that the Ω_c for BECs with repulsive interaction decreases with an increase in the number of atoms [15]. The formation of a vortex and vortex lattice in trapped BECs has been studied and it shows the superfluidity of BEC [16–19]. It has been suggested that the BEC passes through a dynamically unstable stage before the vortex pattern formation [3,20]. The effect of an impulsive force on the instability and hence vortex lattice formation in BECs has also been reported [21].

The experimental study of the stability against collapse has revealed the role of three-body interactions in trapped BECs and these interactions are significant at large scattering lengths [22–24]. The three-body interaction is represented with the quintic nonlinear term in a Gross-Pitaevskii [23–25] equation and its application in the field of nonlinear fiber optics is a well established one [26]. Since the vortex dynamics of the condensate in such systems has not been explored yet, it would be interesting to study the vortex dynamics in such a system both theoretically and experimentally.

Theoretical work on anharmonically trapped BECs with the two-body interactions has been done with variational analysis [27]. Similar studies with the two- and three-body interactions [28] show that the repulsive three-body interactions helps in the formation of the vortex and reduces the critical rotational frequency of the system [28]. However, these theoretical studies are based on a variational method and therefore provide only approximate results. It would therefore be useful to compare the results of these studies with accurate numerical simulations. Since it has already been found that the critical rotation frequency in a harmonically trapped BEC calculated from the thermodynamic arguments does not exactly match with the experimental values [12,27], it will be useful to find the critical rotational frequency numerically. Moreover, studies of vortex lattice formation in the trapped system in the presence of three-body interactions is not reported as yet and it is therefore an interesting problem to analyze the role of such interactions. In this paper we simulate the vortex formation in BECs in the presence of a three-body interaction for both harmonic and anharmonic traps and calculate the critical rotational frequency. The dynamical evolution of the average value of the angular momentum per particle and its relation with the dynamics of the condensate leading to vortex formation is simulated as a function of the two- and three-body interaction parameters and rotational frequency. Our numerical simulation results agree with the earlier theoretical results [28] that the repulsive three-body interaction depresses the critical rotational frequency Ω_c and anharmonicity increases the critical rotation as compared to the case of harmonically trapped BECs. We then simulate the vortex lattice formation in the condensate and study the role of the three-body interaction in the vortex lattice formation.

The paper is organized as follows. In Sec. II, a model for our system is introduced. The time-dependent variational analysis

leading to the theoretical estimate of various parameters of the system, such as the deformation parameter, the average angular momentum per particle, quadrupole frequency, the surface mode frequency, the critical rotational frequency, and their variation with the two- and three-body interaction parameters are reported in this section. In Sec. III, we present the results obtained from numerical simulation of the two-dimensional cubic-quintic Gross-Pitaevskii equation. Finally we conclude in Sec. IV.

II. MODEL

As a model we consider the two-dimensional (2D) cubic-quintic Gross-Pitaevskii (GP) equation given by [29]

$$i\psi_t = -\tfrac{1}{2}(\psi_{xx}+\psi_{yy}) + V(x,y)\psi + i\Omega(x\psi_y - y\psi_x) + p|\psi|^2\psi + q|\psi|^4\psi, \quad (1)$$

where $V(x,y) = \frac{1}{2}[(x^2+y^2)+\lambda(x^2+y^2)^2]$ and Ω are the trapping potential and rotational frequency, respectively. For the harmonic case the small anharmonic term is $\lambda = 0$. Here $p = \frac{g_1 N}{\hbar\omega_\perp a_0^3}$, $q = \frac{g_2 N^2}{\hbar\omega_\perp a_0^6}$, and $a_0 = \sqrt{\frac{\hbar}{m\omega_\perp}}$, where N, g_1, and g_2 denote the total number of particles, and two- and three-body interaction coupling constants, respectively. The spatial coordinates, time, condensate wave function, and rotational frequency are in units of a_0, $\omega_\perp^{-1}$, $a_0^{-3/2}$, and $\omega_\perp$, respectively. Also the condensate wave function ψ is normalized as $\int \psi^*\psi\, dx\, dy = 1$.

The Lagrangian density corresponding to Eq. (1) is given by

$$Ł = \frac{i}{2}(\psi\psi_t^* - \psi^*\psi_t) + \frac{1}{2}|\nabla\psi|^2 + V(x,y)|\psi|^2 + \frac{p}{2}|\psi|^4 + \frac{q}{3}|\psi|^6 - \Omega\psi^* L_z\psi. \quad (2)$$

The effective Lagrangian can be obtained from Eq. (2) as $L = \int_{-\infty}^{\infty} Ł\, dx\, dy$. For studying the properties of a harmonically trapped rotating condensate we use the time-dependent variational analysis. We use Gaussian ansatz for the condensate wave function [2]:

$$\psi(x,y,t) = c(t)e^{-1/2[\alpha(t)x^2+\beta(t)y^2-2i\gamma(t)xy)]}, \quad (3)$$

where $c(t)$ is normalized as $c(t) = (\frac{\sqrt{D}}{\pi})^{1/2}$ and $D = \alpha_1\beta_1 - \gamma_2^2$. Here the complex dimensionless parameters have the form $\alpha(t) = \alpha_1(t) + i\alpha_2(t)$, $\beta(t) = \beta_1(t) + i\beta_2(t)$, and $\gamma(t) = \gamma_1(t) + i\gamma_2(t)$, and the inverse of α_1 and β_1 give the square of the condensate width in the x and y directions, respectively. The Gaussian wave function [Eq. (3)] cannot describe a condensate with a vortex as the phase corresponds to an irrotational flow [30]. Vortices are nucleated when the rotation resonantly excites the quadrupole modes of the condensate and induce large amplitude oscillations (surface mode excitations) of the condensate, resulting in a dynamical instability. Once the system starts deforming, it starts transferring angular momentum to the condensate leading to vortex nucleation, and finally a single vortex is formed when the transferred average angular momentum per particle is 1.

To obtain the relation between the average angular momentum per particle and the shape deformation of the system, we calculate the average of the angular momentum operator $\langle L_z\rangle = \langle xp_y - yp_x\rangle$ using the Gaussian condensate wave function [Eq. (3)] and obtain [27,28]

$$\langle L_z\rangle = \frac{\Omega(1-\eta)^2}{2\eta(\alpha_{10}+\beta_{10})}, \quad (4)$$

where η denotes the shape deformation parameter of the condensate defined as

$$\eta = \frac{\langle x^2\rangle}{\langle y^2\rangle} = \frac{\beta_{10}}{\alpha_{10}} = \frac{\Omega+\gamma_{20}}{\Omega-\gamma_{20}}, \quad (5)$$

and α_{10}, β_{10}, and γ_{20} are the equilibrium values of the variational parameters which can be obtained by minimizing the variational energy [27,28]. Since η is always positive, this implies $\Omega > \gamma_{20}$. Equation (4) shows how the angular momentum transfers to the condensate due to spontaneous shape deformations ($\eta \neq 1$). To reveal dynamical instability and to calculate the quadrupole mode and surface mode frequencies, we take initially a small deviation of the variational parameters from its equilibrium values (keeping only second order deviations) and get coupled linear equations of motion for the deviations. The solutions of these coupled equations give the required frequencies [30]. The quadrupole mode ($m_z \pm 2$) frequency so obtained is given by [28]

$$\omega_q = \sqrt{4 - PR_0^2 - 2QR_0^3}, \quad (6)$$

In the presence of rotation the centrifugal term ($-\Omega L_z$) shifts the quadrupole mode frequency [Eq. (6)] by $\pm 2\Omega$. The lowest energy surface mode frequency is then given by

$$\omega_{-2} = \sqrt{4 - PR_0^2 - 2QR_0^3} - 2\Omega, \quad (7)$$

where R_0 is obtained from the equation $(1 + \frac{P}{2} + QR_0)R_0^2 - 1 = 0$, $P = p/\pi$, and $Q = 4q/9\pi^2$.

From Eqs. (6) and (7) we can see that for $\Omega = \frac{\omega_q}{2}$, the lowest energy surface mode frequency is zero. The system is irrotational until $\Omega = \frac{\omega_q}{2}$, although we are rotating the system. In other words, the system does not respond to the external rotation until $\Omega = \frac{\omega_q}{2}$. Spontaneous symmetry breaking (deformation parameter $\eta \neq 1$) and hence transfer of angular momentum [Eq. (4)] leading to vortex formation happens only for $\Omega > \omega_q/2$. The plot of η vs Ω actually shows that $\eta = 1$ for $0 < \Omega < \frac{\omega_q}{2}$ and there is surface deformation ($\eta \neq 1$) for $\Omega > \frac{\omega_q}{2}$ [27,28]. Figure 1 shows the plot of the quadrupole mode frequency against q for a fixed p. From this

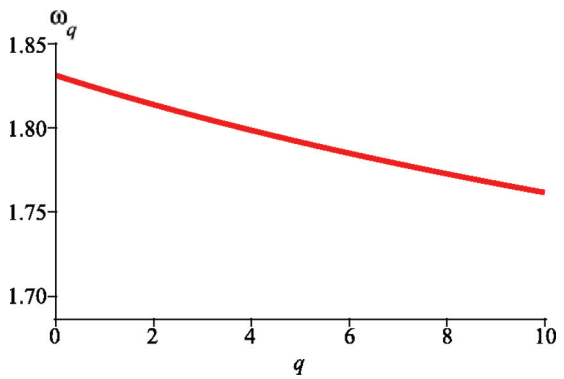

FIG. 1. (Color online) Quadrupole mode frequency ω_q plotted against q for $p = 3$.

figure it follows that the critical rotational frequency $\Omega_c = \frac{\omega_q}{2}$ decreases with an increase in strength of the three-body interaction (q).

III. VORTEX DYNAMICS

Recently Muruganandam *et al.* [31] have shown that the split-step imaginary-time propagation method yields very precise results when compared to the real-time propagation method at low computational cost and is quite appropriate for the solution of stationary problems involving the ground state. So here we perform the numerical simulation of Eq. (1) using the imaginary-time propagation method, where real time t is replaced as $t \to -it$ and the equation is discretized by using the Crank-Nicolson scheme [32]. For our simulation, we take the the initial wave function as Gaussian. For the stable ground state we fix that the interactions are initially absent.

For the time iteration, we split our Eq. (1) into three parts. These are

$$i\psi_t = V(x,y)\psi + p|\psi|^2\psi + q|\psi|^4\psi, \tag{8a}$$

$$i\psi_t = -\tfrac{1}{2}(\psi_{xx}) - i\Omega y\psi_x, \tag{8b}$$

$$i\psi_t = -\tfrac{1}{2}(\psi_{yy}) + i\Omega x\psi_y. \tag{8c}$$

We first solve Eq. (8a) with a given initial value $\psi(x,y,t_0)$ at $t = t_0$. This step provides the solution ψ at an intermediate step $t = t_0 + \Delta$, where Δ is the time step. This intermediate solution is used as the initial value to solve Eqs. (8a) and (8b) for getting the solution at the final time [31]. For our simulation, we set small spatial step $h_x = h_y = 0.04$ and time step $\Delta = 0.01$.

A. Single vortex

According to the experimental results [33], the average angular momentum per particle is one when there is a single vortex created. We show from our simulation that the time evolution of the expectation value of angular momentum L_z reaches the value 1 during a single vortex formation. Figure 2(a) shows the density plot as it evolves in time and Fig. 2(b) shows the variation of the average angular momentum per particle with time during a single vortex formation. From these two figures we can see that, as experimentally observed, $\langle L_z\rangle$ saturates to the value 1 when a single vortex is created as seen from the time variation of the density plot. Meanwhile, the nonzero value of L_z (between 0 and 1) shows the spontaneous shape deformation of the condensate [34]. The saturation of the $\langle L_z\rangle$ value to 1 represents the stability of the single vortex over time. We have obtained the critical rotational frequencies Ω_c for the single vortex formation for different values of the interaction parameters p and q from the numerical simulation of the 2D GP equation [Eq. (1)]. The numerical values of Ω_c for harmonically trapped ($\lambda = 0$) condensates are given in Table I. These values show that Ω_c get depressed by the addition of a repulsive three-body interaction. Figure 3 shows that at critical rotational frequency $\Omega_c = 0.966$ for $p = 1$ and $q = 0$, the average angular momentum per particle reaches 1. From the figure we can see that for $\Omega < \Omega_c$ the average value of L_z is always <1 and consequently no vortex can form. Similarly, the figure shows that for $\Omega > \Omega_c$ a vortex forms much faster in time as the value of $\langle L_z\rangle$ reaches saturation earlier in time. The very accurate nature of our numerical simulation brings

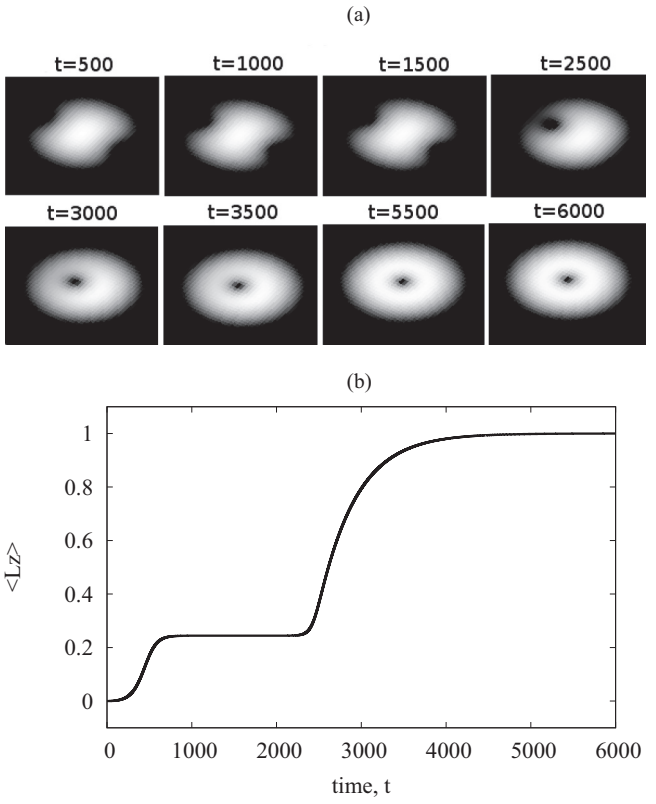

FIG. 2. Time evolution of (a) the condensate density and (b) the average angular momentum per particle, during the single vortex formation for $p = 1$, $q = 3$, and $\Omega = 0.947$.

out the very sensitive dependence of the critical rotational frequency on the dynamics of vortex formation as seen from Fig. 3. The corresponding figures for the $p = 1$ and $q \neq 0$ cases are similar to Fig. 3 and hence are not plotted here. However, the corresponding values of Ω_c for the $p = 1$ and $q \neq 0$ cases as obtained from numerical simulations are given in Table I. Figure 2 is plotted for the rotational frequency $\Omega = 0.947$, which is greater than the corresponding critical rotational frequency $\Omega_c = 0.944$ (see Table I). A comparison of Fig. 2(b) and the curve for $\omega > \Omega_c$ in Fig. 3 shows that in both cases $\langle L_z\rangle$ have intermediate values between 0 and 1 over time. This implies that for the $\Omega > \Omega_c$ case also the condensate undergoes deformations before the formation of the stable single vortex. The horizontal line for the intermediate value of $\langle Lz\rangle$ shows that the vortices stay at the edges for some time before moving to the center of the condensate. Finally, the

TABLE I. Critical rotational frequencies.

λ	p	q	Numerical Ω_c
0	1	0	0.966
	1	3	0.944
	1	5	0.934
0.01	1	0	0.991
	1	3	0.971
	1	5	0.961

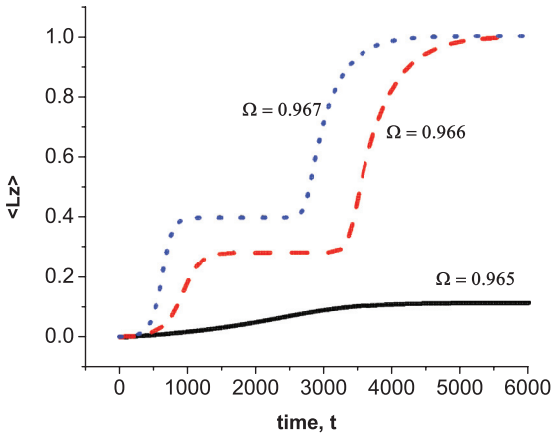

FIG. 3. (Color online) Variation of the average angular momentum per particle for $p = 1$ and $q = 0$ with rotational frequencies.

stable single vortex is formed when $\langle L_z \rangle$ attains the saturation value 1 as shown in Figs. 2(b) and 3.

In order to study the effect of anharmonicity of the trapping potential on the critical rotational frequency Ω_c, we consider a quadratic-plus-quartic trapping potential of the form $V(x,y) = \frac{1}{2}[(x^2+y^2)+\lambda(x^2+y^2)^2]$, where λ is the anharmonic term. Table I gives the details about the critical rotational frequency values obtained through the numerical simulations for $\lambda = 0.01$. From the table we can see that, as in the case of a harmonic trap, the three-body interaction depresses the critical rotational frequency. Also, a comparison between the harmonic and anharmonic cases (Table I) shows that the critical rotational frequencies are quite enhanced for the anharmonic trap as compared to the harmonic trap. This is shown in Fig. 4 for various values of the three-body interaction strength. These observations show that our simulation results are in agreement with the nature of variation of the critical rotational frequency with anharmonicity as obtained theoretically using the variational analysis [28].

The calculations based on the field theory reveal that the three-body interaction (g_2) is a complex quantity because of the three-body recombination effect [35]. The recent experiments on the alkali-metal atoms such as ^{87}Rb and ^{85}Rb show that the imaginary part of g_2 is negligible when compared to the real part, where $\mathrm{Re}(g_2) \approx (10^{-27}$–$10^{-26})\hbar\,\mathrm{cm}^6\,\mathrm{s}^{-1}$. The calculation of dimensionless parameters p and q based on the data for alkali-metal atoms show that the q can be set larger than or less than p [36]. The experiments on alkali-metal atoms show that the three-body interactions are significant only at high densities. Nowadays this can be achieved through the strong confinement of the atoms. The small values of two- and three-body interaction parameters p and q, respectively, chosen above is for the case when the total number of particles in the trap is small. We now increase the number of trapped particles and take it as $N = 10^4$ in agreement with the available experimental data of alkali-metal atoms. For this value of N, the two- and three-body interaction parameter values turns out to be $p \approx 580$ and $q \approx 80$–900 for ^{87}Rb. For this value of the parameter p, numerical simulation shows that $\Omega_c \approx 0.425$ for the range of q ($q \approx 80$–900). This implies that the critical rotational frequency is not affected by the variation of the the strength of three-body interactions and is apparently in contradiction to our variational results as mentioned above. In order to understand the reason behind this, we calculated the quadrupole mode frequency for higher values of the dimensionless two-body interaction parameter p. The plot of quadrupole mode frequency in Fig. 5 shows that a significant decrease in its values occurs only when the strength of the two-body interactions is small. However, for a large value of parameter p [$p = 580$ in Fig. 5], we find that Ω_q (hence Ω_c) remains almost constant with variations of q showing agreement of the variational result with the numerical simulation.

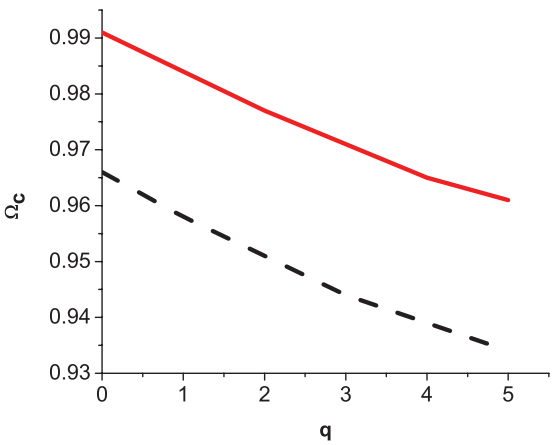

FIG. 4. (Color online) Variation of critical rotational frequency with q for $p = 1$. The solid line corresponds to $\lambda = 0.01$ and the dashed line is for $\lambda = 0$.

B. Vortex lattice

Figure 6 shows the time evolution of vortex lattice pattern formation in a harmonic trap for the case $q > p$. The first and second panels of Fig. 6 are for intermediate time dynamics at $t = 500$ and $t = 1500$, respectively, showing that even though the vortex lattice structures are almost formed, the vortices are still entering the condensate through the boundary. The third panel at $t = 7500$ shows the final stable vortex lattice structure. We observe a similar final stable vortex pattern for the cases $p = q$ and $q < p$ also, but the intermediate time pattern may

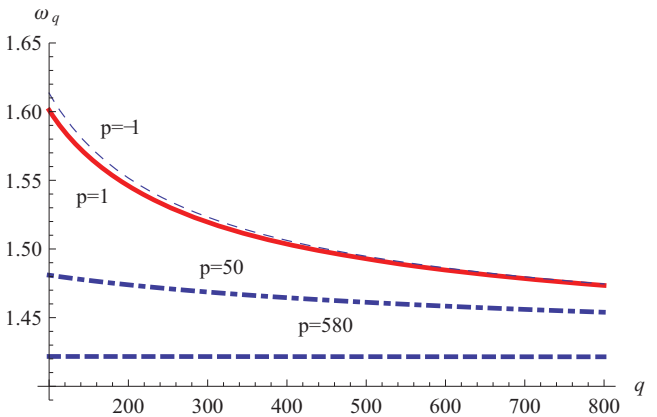

FIG. 5. (Color online) Plot of quadrupole mode frequency ω_q against q for different p.

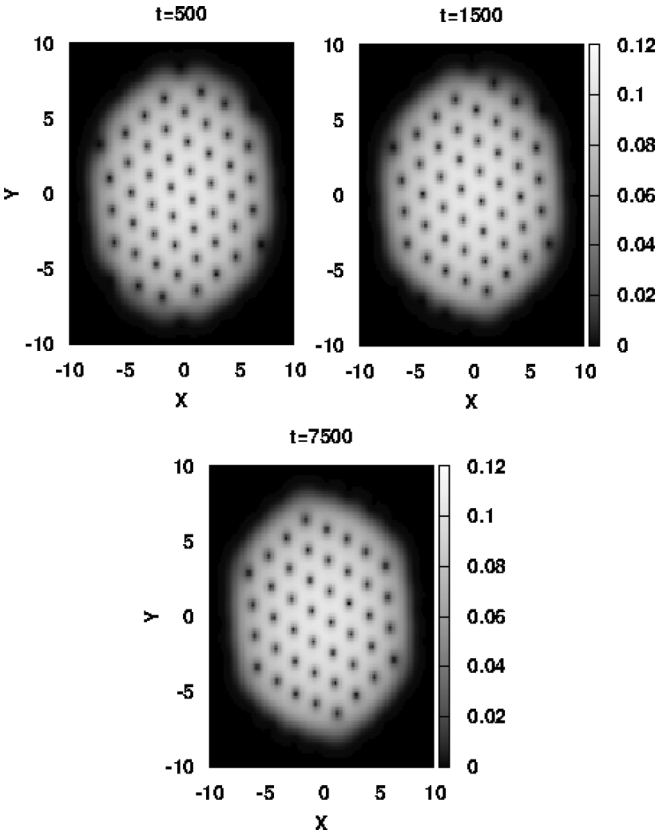

FIG. 6. Density plot of vortex lattice formation for the case $p = 580$, $q = 890$, and $\Omega = 0.92$. Here the figures are at $t = 500$, 1500, and 7500.

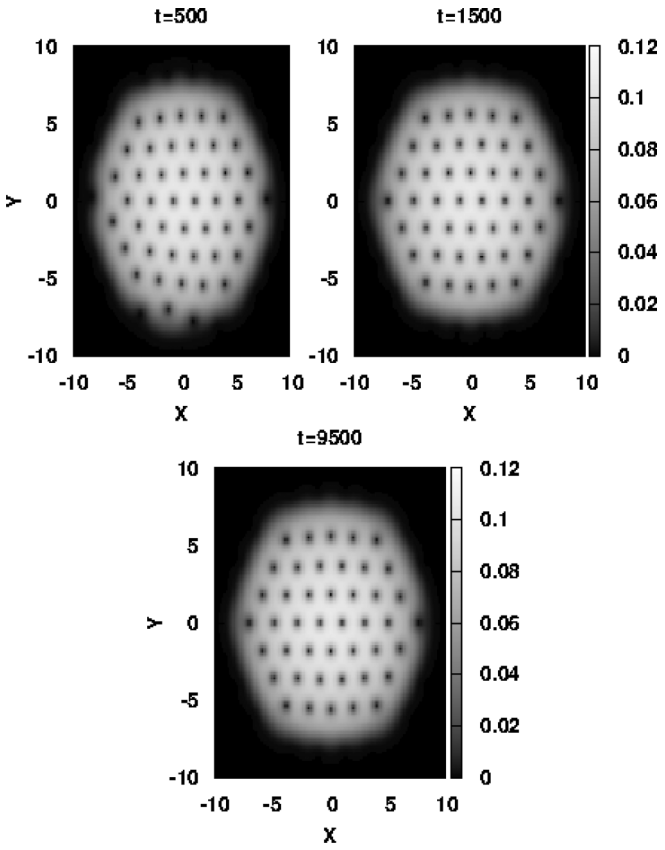

FIG. 7. Density plot of vortex lattice formation for the case $p = 580$, $q = -890$, and $\Omega = 0.92$. Here the figures are at $t = 500$, 1500, and 9500.

be different. As the harmonically trapped cubic case ($q = 0$) favors a triangular lattice [16], we can see that the three-body interaction also favors the same lattice arrangements.

The vortex lattices with repulsive two-body and attractive three-body interactions are shown in Fig. 7. The first panel of Fig. 7 for intermediate time dynamics at $t = 500$ shows that the vortices are entering the condensate through the boundary, whereas the second panel at $t = 1500$ shows that number of vortices entering the condensate has decreased considerably. The third panel below for longer time ($t = 9500$) shows the stable vortex lattice. These figures are very similar to Fig. 6 showing that the nature of the three-body interaction, whether it is repulsive or attractive, does not alter the vortex lattice arrangements, but the time to form the final stable vortex lattice is different for different cases. The existence of a stable vortex lattice for the $p > 0$ and $q < 0$ cases as shown above (Fig. 7) has similarity with the results of Song and Li [8] where they showed that stable vortex-soliton solutions are also allowed for repulsive two-body and attractive three-body interactions.

The vortices arrangement for the attractive two-body and repulsive three-body case is depicted in Fig. 8. Here the two-body interaction parameter p is taken to be small as higher values of p lead to instability of the condensate. This figure shows that if the strength of the repulsive three-body interaction is higher than the attractive two-body, vortices can appear even in the repulsive two-body attractive system also.

Finally, we checked the possibility of formation of vortices in a purely three-body interactive system. Such condensates have already been produced experimentally [37,38]. We observe the same vortex lattice pattern as in Fig. 8. The vortex lattice formation for the anharmonic trap also follows the same lattice arrangements of vortices.

Figure 9 shows that for the same number of vortices (which is three in this case), the time of vortex nucleation decreases with an increase in strength of the repulsive three-body interaction. On the other hand, for the attractive interaction case, the time of vortex nucleation increases with an increase

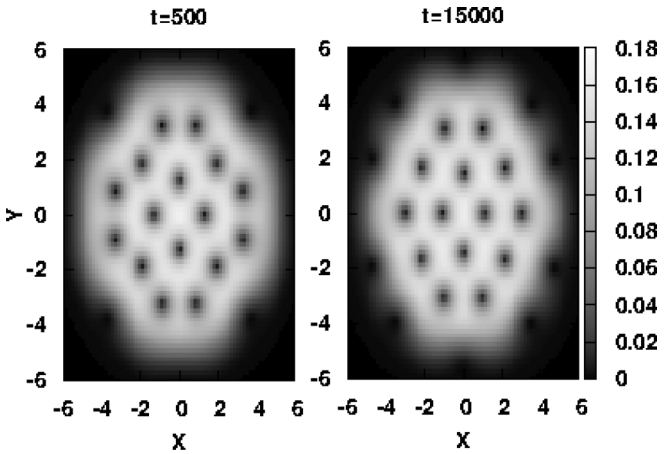

FIG. 8. Density plot of vortex lattice formation for the case $p = -0.5$, $q = 800$, and $\Omega = 0.98$.

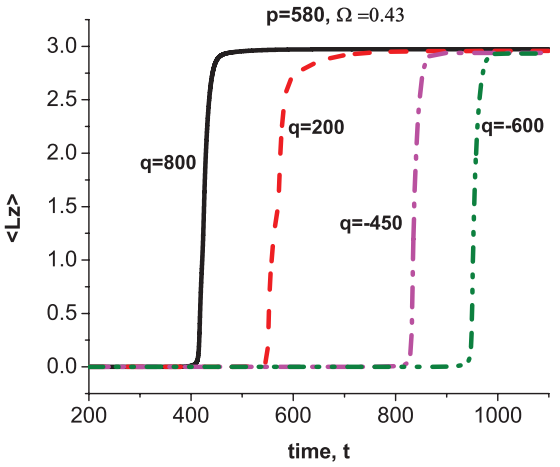

FIG. 9. (Color online) Variation of the average value of the angular momentum with time for attractive and repulsive q at $p = 580$.

in strength of the attractive three-body interaction. Also it is observed that time for vortex nucleation is smaller for the repulsive three-body interaction as compared to the attractive three-body interaction. An interesting observation is that the number of vortices is reduced when the strength of the repulsive three-body interaction approaches the strength of the repulsive two-body interaction. This is shown in Fig. 10. Here $\Omega = 0.43$ and is near to Ω_c. The number of vortices is three for $p = 580$ and $q = 200$. But for $q = 500$ the number of vortices is reduced to two. A further increase in q going beyond the value of p shows that the number of vortices is again increased to three. This effect is absent when $\Omega \gg \Omega_c$ and also for attractive three-body interaction. This interesting observation can be used as a mechanism to control the number of vortices in the system.

IV. CONCLUSION

We have studied vortex dynamics in BECs with tunable two- and three-body interactions and explored the role of three-body interactions on single vortex and vortex lattice formation. We have used parameter values for the two- and three-body interactions which correspond to the experimental parameters of the BEC. The number of vortices that appear depends on the parameters of the simulations p, q, and Ω.

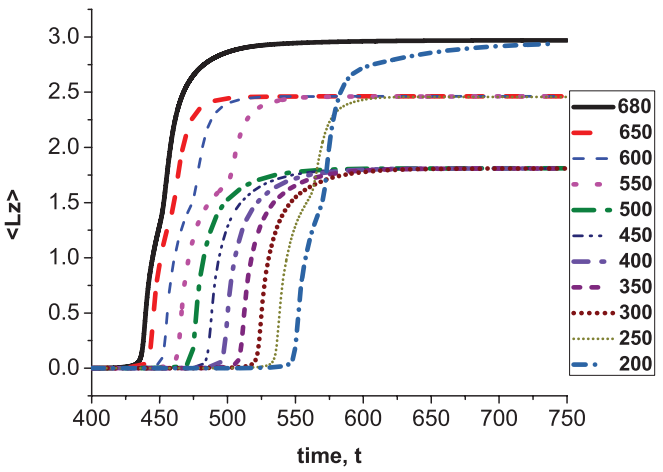

FIG. 10. (Color online) Variation of the average value of the angular momentum with time for different q. Here $p = 580$ and $\Omega = 0.43$.

Our numerical simulation results show that for BECs confined in a harmonic trap, the repulsive three-body interaction depresses the critical value of rotational frequency which is in agreement with our time-dependent variational analysis and also earlier theoretical studies [28]. But for BECs confined in an anharmonic trap, the anharmonicity increases the value of the critical rotational frequency when compared to a harmonically trapped BEC. However, its value is lowered in the presence of the three-body interaction. Also our results show that the time of formation of vortices decreases with an increase in rotational frequency values above Ω_c. Similarly, the vortex forms much faster in time with an increase of the strength of the repulsive three-body interaction. This is in contrast to the attractive three-body interaction case where the vortex nucleation time increases with increasing strength of the attractive three-body interaction. The numerical simulation for the vortex lattice formation shows that the magnitude of three-body interaction does not alter the vortex pattern and also it does not depend on the type of three-body interaction (attractive or repulsive), but the type of interaction affects the number of vortices when Ω is near to Ω_c. This mechanism can be used to control the number of vortices in BECs.

The vortex formation in the harmonically trapped purely attractive cubic BEC is restricted because of the lack of shape deformation [14,27]. But our results show that the addition of a repulsive three-body interaction with magnitude larger than the attractive two-body interaction enables the shape deformation and leads to the vortex formation. Our numerical simulation shows that the vortex formation in purely quintic BECs is also possible. The vortex patterns as obtained with different interaction strengths show that irrespective of the types of interactions, whether two-body or three-body, the BECs favor a triangular vortex lattice.

Recent theoretical studies have shown that the Gross-Pitaevskii equation can be modified with a higher order term $(\nabla^2|\psi|^2)\psi$, where corrections in the effective range of two-body interactions are needed [39]. The cases such as Rydberg molecules embedded in BECs and narrow Feshbach resonances are certain examples [40]. Our variational analysis using the Gaussian wave function given in Eq. (3) shows that the equation determining the quadrupole mode frequency for the modified GP equation as mentioned above is the same as in Eq. (6). The details of the analysis will be published elsewhere. This shows that the effect of higher order corrections resulting from the effective range corrections and the three-body interactions have a similar effect on the critical rotational frequencies for the vortex formation in BECs.

ACKNOWLEDGMENTS

B.D. thanks DST for financial support through a research project. K.P. thanks DST, DAE-BRNS, CSIR, and UGC for the financial support through research projects. T.M. is thankful to A. Kibey and R. Sonone for their support.

[1] M. R. Matthews, B. P. Anderson, P. C. Haljan, D. S. Hall, C. E. Wieman, and E. A. Cornell, Phys. Rev. Lett. **83**, 2498 (1999).
[2] J. R. Abo-Shaeer, C. Raman, J. M. Vogels, and W. Ketterle, Science **292**, 476 (2001).
[3] K. W. Madison, F. Chevy, W. Wohlleben, and J. Dalibard, Phys. Rev. Lett. **84**, 806 (2000).
[4] F. Dalfovo, C. Minniti, and L. P. Pitaevskii, Phys. Rev. A **56**, 4855 (1997).
[5] G. Hechenblaikner, O. M. Marago, E. Hodby, J. Arlt, S. Hopkins, and C. J. Foot, Phys. Rev. Lett. **85**, 692 (2000).
[6] C. Lee, J. Huang, H. Deng, H. Dai, and J. Xu, Front. Phys. **7**, 109 (2012).
[7] D. Wang, X. Zeng, and Y. Ma, Phys. Lett. A **376**, 3067 (2012).
[8] X. Song and H. Li, Phys. Lett. A **377**, 714 (2013).
[9] L. D. Landau, J. Phys. (Moscow) **5**, 71 (1941).
[10] E. L. Bolda and D. F. Walls, Phys. Lett. A **246**, 32 (1998).
[11] C. Raman, J. R. Abo-Shaeer, J. M. Vogels, K. Xu, and W. Ketterle, Phys. Rev. Lett. **87**, 210402 (2001).
[12] M. Krämer, L. Pitaevskii, S. Stringari, and F. Zambelli, Laser Phys. **12**, 113 (2002).
[13] P. Rosenbusch, D. S. Petrov, S. Sinha, F. Chevy, V. Bretin, Y. Castin, G. Shlyapnikov, and J. Dalibard, Phys. Rev. Lett. **88**, 250403 (2002).
[14] S. Stringari, Phys. Rev. Lett. **77**, 2360 (1996).
[15] F. Dalfovo and S. Stringari, Phys. Rev. A **53**, 2477 (1996).
[16] R. Zeng and Y. Zhang, Comput. Phys. Commun. **180**, 854 (2009).
[17] A. Aftalion and Q. Du, Phys. Rev. A **64**, 063603 (2001).
[18] O. K. Vorov, P. Van Isacker, M. S. Hussein, and K. Bartschat, Phys. Rev. Lett. **95**, 230406 (2005).
[19] L. H. Wen and X. B. Luo, Laser Phys. Lett. **9**, 618 (2012).
[20] D. L. Feder and C. W. Clark, Phys. Rev. Lett. **87**, 190401 (2001).
[21] S. K. Adhikari and P. Muruganandam, Phys. Lett. A **301**, 333 (2002).
[22] A. Gammal, T. Frederico, and L. Tomio, Phys. Rev. E **60**, 2421 (1999).
[23] T. Kohler, Phys. Rev. Lett. **89**, 210404 (2002).
[24] A. Gammal, T. Frederico, L. Tomio, and F. Kh. Abdullaev, Phys. Lett. A **267**, 305 (2000).
[25] P. Pieri and G. C. Strinati, Phys. Rev. Lett. **91**, 030401 (2003).
[26] S. Gatz and J. Herrmann, Opt. Lett. **17**, 484 (1992).
[27] T. K. Ghosh, Phys. Rev. A **69**, 043606 (2004).
[28] M. Juan, L. Zhi, and X. Ju-Kui, Chin. Phys. B **18**, 4122 (2009).
[29] W. Bao, Q. Du, and Y. Zhang, SIAM J. Appl. Math. **66**, 758 (2006).
[30] S. Sinha and Y. Castin, Phys. Rev. Lett. **87**, 190402 (2001).
[31] P. Muruganandam and S. K. Adhikari, Comput. Phys. Commun. **180**, 1888 (2009).
[32] S. E. Koonin and D. C. Meredith, *Computational Physics: Fortran Version* (Addison-Wesley, Reading, 1990).
[33] F. Chevy, K. W. Madison, and J. Dalibard, Phys. Rev. Lett. **85**, 2223 (2000).
[34] R. K. Kumar and P. Muruganandam, J. Phys. B **45**, 215301 (2012).
[35] E. Braaten and A. Nieto, Eur. Phys. J. B **11**, 143 (1999).
[36] H. Al-Jibbouri, I. Vidanovic, A. Balaz, and A. Pelster, J. Phys. B **46**, 065303 (2013).
[37] T. Kramer *et al.*, Nature (London) **440**, 315 (2006).
[38] A. Safavi-Naini, J. von Stecher, B. Capogrosso-Sansone, and Seth T. Rittenhouse, Phys. Rev. Lett. **109**, 135302 (2012).
[39] A. Collin, P. Massignan, and C. J. Pethick, Phys. Rev. A **75**, 013615 (2007).
[40] M. Thøgersen, N. T. Zinner, and A. S. Jensen, Phys. Rev. A **80**, 043625 (2009).